Composition Gradient High-Throughput Polymer Libraries Enabled by Passive Mixing and Elevated Temperature Operability

Aaron L. Liu,[a]† Ezgi M. Dogan-Guner,[a]† Michael McBride,[a] Rahul Venkatesh,[a] Miguel Angel Gonzalez,[a] Elsa Reichmanis,[b] Martha Grover,[a*] J. Carson Meredith[a*]*

† These authors contributed equally to this work.

[a]School of Chemical & Biomolecular Engineering, Georgia Institute of Technology, 311 Ferst Drive, Atlanta, GA, 30332

[b]Department of Chemical & Biomolecular Engineering, Lehigh University, Bethlehem, PA, 18015

*Authors to whom correspondence should be addressed: carson.meredith@chbe.gatech.edu, martha.grover@chbe.gatech.edu, elr420@lehigh.edu

ABSTRACT

The development of high-throughput experimentation (HTE) methods to efficiently screen multiparameter spaces is key to accelerating the discovery of high-performance multicomponent materials (*e.g.*, polymer blends, colloids, etc.) for sensors, separations, energy, coatings, and other thin-film applications relevant to society. Although the generation and characterization of gradient thin-film library samples is a common approach to enable materials HTE, the ability to study many systems is impeded by the need to overcome unfavorable solubilities and viscosities among other processing challenges at ambient conditions. In this protocol, a solution coating system capable of operating temperatures over 110 °C is designed and demonstrated for the deposition of composition gradient polymer libraries. The system is equipped with a custom, solvent-resistant passive mixer module suitable for high-temperature mixing of polymer solutions at ambient pressure. Residence time distribution modeling was employed to predict the coating conditions necessary to generate composition gradient films using a poly(3-hexylthiophene) and poly(styrene) model system. Poly(propylene) and poly(styrene) blends were selected as a first demonstration of high temperature gradient film coating: the blend represents a polymer system where gradient films are traditionally difficult to generate *via* existing coating approaches due to solubility constraints at ambient conditions. The methodology developed here is expected to widen the range of solution processed materials that can be explored via high-throughput laboratory sampling and provides an avenue for efficiently screening multiparameter materials spaces and/or populating the large datasets required to enable data-driven materials science.

1. INTRODUCTION

The design of materials and processes for advanced applications such as energy storage[1] and conversion,[2] membrane separations,[3] biosensors,[4] organic electronics,[5] and stretchable devices,[6] often requires formulations comprising multiple layers, composites, or blends in tunable compositions to elicit processibility,[7] structural morphology,[8] and/or final performance.[9] Materials discovery and efficient application development within the vast composition space accessible through multi-material systems, however, is challenging. For instance, when important transitions in polymer phase behavior, microstructure, or related phenomena occur within a narrow window,[10] optimization may require full screening of a complex composition/process landscape.[11] Coupled with the potentially tremendous expense in time and resources required to generate sufficient laboratory sampling, the need to efficiently screen combinatorial parameter spaces motivates the development of high-throughput experimentation (HTE) techniques tailored to materials screening in general,[12] and polymer materials screening in particular.[13] Such methodologies are important tools in accomplishing the data-driven experimental thrusts put forth by the Materials Genome Initiative.[14, 15]

Recent sample generation strategies to enable HTE of polymer materials have included either robotized generation of discrete samples or the supervised deposition of gradient samples.[16] The former set-ups are an attractive autonomous option for accelerated screening but typically involve fabrication-intensive discrete sampling, which may not always be feasible with available infrastructure and resources.[17] Alternatively, gradient methodologies that employ a solution-based coating process and a mixing protocol to deposit a continuous film library with spatially varying compositions, provide a platform for subsequent high-throughput characterization.[18] The advent of solution-based approaches, coupled with a desire to minimize the required analyte and solution volumes has motivated the use of custom mixing components inspired by microfluidic designs.[19-23] Microfluidic devices are easily fabricated in soft materials using photolithographic processes and can minimize solution volume.[24] Because the characteristic laminar flow within microfluidic mixers creates challenges in achieving adequate mixing efficiency,[25] active or passive mixing elements are often introduced into flow systems to provide *in-situ* formulation capabilities.[26] Passive configurations with herringbone grooves along the channel, for example,[27-29] allow the input solutions to be folded multiple times during flow to result in efficient mixing.[25, 30]

Despite advances in small-volume mixing technologies, polymer solubility and high solution viscosities remain as hurdles that must be overcome to implement high-throughput polymer experimentation as a routine methodology. The challenges associated with solubility and viscosity necessitate the use of solvents and/or temperatures that are incompatible with common microfluidic materials and mixer designs. For example, common microfluidic modules fabricated from soft materials (e.g., poly(dimethylsiloxane) (PDMS), poly(methyl methacrylate) (PMMA)) lack requisite chemical resistance to function adequately with many organic solvents and/or thermal stability needed for operation at high temperatures.[31] Glass and silicon microfluidic modules either incorporate a sealing adhesive that may also suffer from the aforementioned chemical and/or thermal stability issues[32] or alternatively require some complex etching and bonding process.[33, 34] As a result, alternative approaches are required since elevated temperature operability is necessary to achieve dissolution or low viscosity.

Further, to reduce the viscosity, dilution of the species of interest may be required to prevent clogging or induce favorable mixing,[19] but dilution may not always be desired when higher

solution concentrations are necessary.[35] A microfluidic design by Roy *et al.* employed an active mixer to perform gradient studies of poly(3,4-ethylenedioxythiophene):polystyrene sulfonate (PEDOT:PSS) in dimethyl sulfoxide (DMSO), but since it only operated at ambient temperatures, dilution of the species of interest was required to prevent clogging.[23] Recent work by Rodriguez-Martinez *et al.* demonstrated the solution deposition of lateral composition gradient polymer films for organic photovoltaics at ambient temperatures featuring the use of a microfluidic passive mixer 3D-printed from a proprietary wax material resistant to chlorinated solvents.[21] However, extension of this design to other polymer systems could be challenging if elevated temperature is required. While An *et al.* reported the use of a heated slot die to study high temperature processing (up to 130 °C) of polymer ternary libraries, heating only occurred at deposition,[36] and thus the approach is incompatible with low solubility materials. Although the above designs demonstrate the viability of applying gradient film methodologies to enable HTE in polymer systems, challenges associated with materials ambient solubility remain. We note that solubility is a common challenge in mobilizing experimental library methods for many materials of interest including a large subset of polymer semiconductors,[37] photoactive materials,[38] colloidal nanocrystals,[39] membrane materials,[40, 41] poly(olefins),[42] and others.

Herein, we present a solution coating method for depositing polymer gradient thin films by incorporating a staggered herringbone mixer design. The passive mixer, fabricated in aluminum as a serpentine channel with herringbone grooves, was employed to induce effective mixing of two polymer solutions and address the solvent and temperature challenges associated with selected polymers. By initially modeling the mixer behavior with residence time distribution (RTD) studies, we demonstrate solution-processed gradient films with a controlled concentration profile using two different polymer systems. First, a gradient film study of a P3HT:PS blend system at ambient conditions is presented to demonstrate the generation of composition gradient thin films. This system is relevant for organic semiconductor applications, where incorporation of a π-conjugated polymer (P3HT) with an insulating polymer (PS) is known to induce morphological changes that affect charge transport.[5, 43] Next, compatibility of the design with elevated temperature operation is demonstrated using polypropylene (PP) with PS. PP can be modified or mixed with fillers and/or other polymers to afford a composite or blend, respectively, to tune its mechanical properties.[44, 45] To our knowledge, these results represent the first reported generation of a library sample requiring elevated temperatures (up to 110 °C) to overcome ambient solubility constraints. We envision that the high temperature capabilities reported here will provide for the adoption of library techniques for a broader range of polymers with ambient solubility constraints.

2. METHODS

2.1. Materials

Poly(3-hexylthiophene) (P3HT) (M_w = 58 kDa, RR = 95%, Rieke Metals, Inc.), polystyrene (PS) (two different samples at M_w = 35 kDa and M_w = 216 kDa, MilliporeSigma), isotactic polypropylene (PP) (M_w = 16 kDa, see **Supporting Information**, WINTEC WMG03UX), maleic anhydride-graft-polypropylene (MA-g-PP) (M_w = 9.1 kDa, maleic anhydride 8-10 wt.%, Sigma-Aldrich), chloroform (MilliporeSigma, anhydrous, amylenes as stabilizer), and o-xylene (MilliporeSigma) were used as obtained. For ambient tracer experiments, colorless initial

solution (100% PS, M_w = 35 kDa) and tracer solution (30:70 P3HT:PS by weight) were dissolved at a total 10 mg/mL polymer concentration in chloroform by stirring in closed 20 mL vials at 55 °C for 60 min, cooled to ambient temperature for 20 min, and used with no further processing for solution tracer measurements.

2.2. Overall Flow Coating Design

A schematic of the flow coating design is depicted in **Figure 1**. This system is an augmentation of the gradient pumping system design.[19] Two computer-controlled syringe pumps (New Era Pump Systems, NE-1000) deliver the polymer solutions into the system, supplied by vertically mounted 9.138 mm diameter stainless steel syringes (New Era Pump Systems, SYR-SS8) (**Figure 1d**). The solutions are infused into a custom-designed static herringbone microfluidic mixing chamber, fabricated from aluminum (**Figure 1a**). This channel mixer has a serpentine herringbone configuration[28-30] consisting of fourteen total mixing elements. Each element consists of ten herringbone-shaped grooves in a staggered five 'left-handed' and five 'right-handed' pattern. The serpentine feature of the channel design is accomplished by incorporating 90° turns after every two mixing elements. Sealing of the mixing module is accomplished by securing a 1/32 inch thick Teflon™ sheet between the mixer and an aluminum cover plate. Downstream of the mixer, a 1/8 inch three-way valve (Swagelok, SS-41GXS2) controls flow to either an outlet purge for effluent collection or to a microchannel distributor mounted to a stainless-steel coating blade (**Figure 1b**). The distributor channel design encourages equal distribution times of solution when deposited at the outlet onto a substrate.[19] The syringes, mixer, and distributor are connected by stainless steel tubing with 1.524 mm inner diameter (High Pressure Equipment, 15-9A2). The total internal volume of the system including the mixer, tubing, and the distributor is approximately 2.05 mL, measured by filling the system with water. Heating control of the system was enabled by jacketing the syringes and tubing with high temperature, heavy insulated heating tapes (BriskHeat, XtremeFLEX®, BWH051020L-60L) and by outfitting the mixer and distributor with thermal cartridges (Omega, HDC00034).

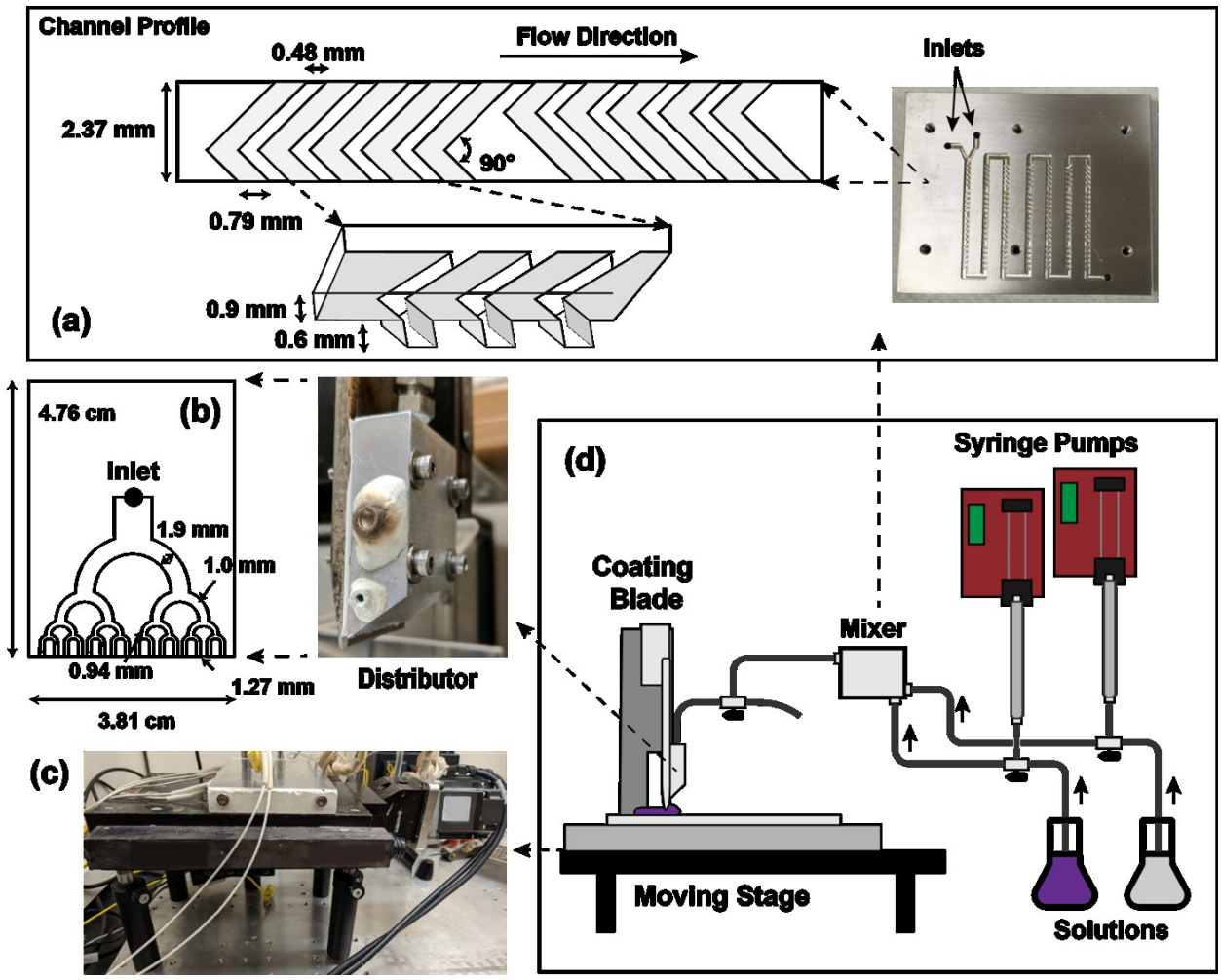

Figure 1. Overview of the gradient film coating system. (a) Image and design of serpentine herringbone mixer module (b) Image and design of microchannel distributor (c) Image of aluminum sample holding stage mounted on motion control (d) Schematic flow diagram of the gradient film coating system

The motion-controlled stage (Parker-Daedal, 106006BT) is outfitted with a computer-controlled AC servo motor (Mitsubishi HG-KR23K). The distributor outlet feeds to a substrate affixed to a heated aluminum surface, which is mounted onto a level-controlled stage by ceramic brackets (**Figure 1c**).

2.3. Tracer Studies

2.3.1. Concentration Profile Generation

To quantify the age (or residence time) distribution of fluid elements within the mixer, tracer measurements were performed as follows.[46] Tracer solution of known concentration was injected into the system as a pulse input, and the time-varying effluent concentration was measured at a constant flow rate. This concentration profile was then analyzed and fit to an RTD model, which was subsequently used to interpret mixer behavior and determine the input flow conditions required to obtain the desired output composition gradient profile.

Initial (100% PS) and tracer (30:70 P3HT:PS) solutions (preparation detailed above) were employed for solution-based tracer measurements. In a pulse tracer experiment, the two syringe pumps were respectively filled with tracer and initial solution, the latter of which was used to initially fill the system. Then, tracer solution was infused into the mixer for five seconds at the given flow rate before again pumping the initial solution at the chosen constant flow rate. Mixer effluent was collected in vials at the purge stream at regular intervals. Tracer experiments were performed in triplicate at flow rates of 20, 60, and 100 mL/hr. To generate the concentration profile, time-dependent effluent concentrations were measured by diluting 40 μL of collected effluent with 2 mL of chloroform in a quartz cuvette with 1 cm pathlength, then taking the characteristic peak height of the UV-vis spectrum (see section 2.5 and **Figure S1, Supporting Information**).

2.3.2. Residence Time Distribution Modeling

The measured effluent concentration profiles obtained from pulse tracer experiments were analyzed as RTD profiles according to Fogler[46] and Himmelblau & Bischoff.[47, 48] For a pulse tracer experiment, the RTD is obtained from the measured time-dependent effluent concentration profile at constant volumetric flow rate (υ) by the following equation:

$$E(t) = \frac{C(t)}{\int_0^\infty C(t)\,dt} \tag{1}$$

where $C(t)$ is the concentration of tracer in the effluent over time (t) and *E(t)* is the RTD, or age distribution of fluid element residence times with the mixer.[48] While the integral of *E(t)* taken to $t \to \infty$ is equal to 1, the first moment of the RTD function gives the apparent mean residence time (τ_a):

$$\tau_a = \int_0^\infty tE(t)\,dt \tag{2}$$

$$\theta = \frac{t}{\tau_a} \tag{3a}$$

$$\tau_0 = \frac{V}{\upsilon} \tag{3b}$$

The time coordinate can then be expressed as the dimensionless time variable θ in Equation 3a. While τ_a should theoretically approach the mixer's space time (τ_0) calculated from the known mixer volume (V) and flow rate (υ) (Equation 3b), measuring the effluent concentration for times longer than $\theta >$ ~2-3 times the mean residence time to reach this theoretical agreement is not always experimentally feasible.[47] Tracer experiments were generally truncated at $\theta = 2.0$, which generally corresponded to the approximate processing time required for gradient thin film coating in this study.

The time-dimensionless form of the RTD measurement *E(θ)*, obtained through Equations 1 and 3, was used to evaluate the mixer behavior, Equation 4. Model parameters for the Tank-in-Series (TIS) and multibranch (MBM) models were obtained by fitting the *E(θ)* profiles using a Nelder-Mead algorithm implemented in Python.[49] Two different models were considered: TIS and MBM. The TIS model approximates the system between the limits of a continuous stirred-tank reactor (CSTR) and a plug flow reactor (PFR), or perfect mixing behavior and no mixing behavior,

respectively. The system is modeled as a series of n perfectly mixed CSTRs of equal volume, where the mixer approaches PFR behavior as $n \to \infty$.[47]

$$E(\theta) = \frac{n^n}{(n-1)!}\theta^{n-1}e^{-n\theta} \tag{4}$$

Common non-ideal flow aspects that are not accounted for in Equation 4 include bypassing and dead volume, where some fraction of fluid elements either spend less or more time, respectively, than the average residence time.[48] To account for these factors, a MBM proposed by Himmelblau and Bischoff[47] was employed:

$$E(\theta) = f\frac{n^n}{(n-1)!}\beta^n\theta^{n-1}e^{-n\beta\theta} + (1-f)\frac{m^m}{(m-1)!}\left(\frac{\beta}{\alpha}\right)^m\theta^{m-1}e^{-\frac{m\beta\theta}{\alpha}} \tag{5}$$

$$\alpha = \frac{\tau_{main}}{\tau_{side}} \tag{6}$$

$$\beta = f + (1-f)\alpha \tag{7}$$

The MBM model (Equation 5) represents the mixing system as two parallel streams, each containing a series of ideal mixers. One branch represents the main flow as ideal mixing in most of the mixer volume. The other branch, the side branch, characterizes the volume of non-ideal fluid elements that contribute dead volume or bypassing behavior. In Equation (5), n and m are the numbers of CSTRs in the side branch and main branch, respectively. Additionally, f stands for the fraction of total fluid flow to the non-ideal side branch; the model simplifies to the TIS model as $f \to 0$, while $0 < f < 1$ signals a greater departure from the TIS model and greater contribution from non-ideal flow elements. The α is the ratio of mean residence times of the main and side branches (Equation 6) and identifies the general non-ideal behavior as bypassing or dead volume. A value of $\alpha \leq 1$ means that the side branch retains some fluid elements opposed to the main stream, indicating presence of dead volume. If $\alpha \geq 1$, some fluid elements pass through the mixer much more rapidly, indicating the presence of bypassing. Defined in Equation (7), β is introduced in the original derivation to simplify the representation of the model equation.[47]

The RTD profiles $E(t)$ as introduced above were collected from pulse inputs for analysis, but step inputs were used to generate actual gradient composition profiles. A prediction of the effluent profile from a step input is enabled by calculating the cumulative RTD function $F(t)$ from $E(t)$:

$$F(t) = \int_0^t E(t)\,dt \tag{8}$$

When a step input is applied, $F(t)$ (which varies from 0 to 1) describes the effluent composition as it progresses from that of the initial solution to the final solution. At a given constant flow rate, Equation 8 provides a predicted flow profile for depositing a gradient thin film, which can be scaled by the composition or concentration of the final solution.

2.4. Film Sample Preparation

2.4.1. P3HT:PS gradient films

P3HT:PS solutions were first dissolved as described above, and then further pre-processed by UV-irradiation using a handheld lamp (Entela, Model UVGL-15, 5 mW cm^{-2}, 254 nm) for 8 minutes according to the procedure in Chang et al[43] and aged for 7 days to promote solution aggregation. Glass substrates (Electron Microscopy Sciences) were cleaned by sequential sonication in acetone, methanol, and isopropanol (20 min each), followed by cleaning in UV–ozone for 30 min (Novascan PSD-UV). The syringes feeding the flow system were filled with P3HT:PS and PS solutions, respectively. Prior to coating, the mixer was initially infused with PS solution. A step input of P3HT:PS solution (constant flow rate of 20 mL/h) was continuously infused into the system. Flow was directed to the purge value to collect effluent for 150 s before diverting flow to the distributor. The outlet solution was blade coated at 2.5 mm/s at a stage temperature of 50 °C. When the available substrate length (60 mm) exceeded that required for the desired coating length, pump flow was paused, stage position reset, and a new substrate affixed before flow was resumed.

2.4.2. PP:PS gradient films

For compatibilized PP:PS gradient films, 95:5 PP/MA-g-PP and 95:5 PS/MA-g-PP (ratios by weight) solutions in o-xylene were blended by combining the required amounts of PP, PS (M_w = 216 kDa), MA-g-PP, and o-xylene at a total concentration of 50 mg/mL. Solutions were stirred at 120 °C for at least 60 min or until completely dissolved, and then used as the feed solutions for gradient thin film generation. The blend fraction x_{PS} refers to the weight percent of PS relative to the total weight of components excluding the compatibilizer:

$$x_{PS} = \frac{m_{PS}}{m_{PS}+m_{PP}} \tag{9}$$

For solution coating, all system component temperatures were maintained at 110 °C. Prior to coating, the mixer was initially infused with PP/MA-g-PP solution. A step input of PS/MA-g-PP solution (constant flow rate of 100 mL/h) was continuously infused into the system. For a single-film gradient, flow was purged for 15 s before depositing solution on a glass substrate at 1.0 mm/s for 60 s with a stage temperature of 110 °C. A separate experiment deposited the effluent of a step input without purging, coating solution across two glass substrates over a total of 120 s. Film samples were cured on the stage for 10 min to remove excess solvent. Free-standing films were recovered by immersing films in DI water to facilitate peel-off from the substrate.

2.5. Characterization of solution and thin film samples

UV-vis spectra for tracer measurements were collected in transmission mode using a Cary 60 UV-vis spectrophotometer.

X-ray photoelectron spectroscopy (XPS) was performed on P3HT thin-film samples using a Thermo K-Alpha XPS system equipped with a monochromatic Al-K X-ray source (1468 eV). Spectra were collected using a flood gun with high purity Argon gas and an X-ray spot size of 400 μm. Survey scans were collected with pass energy of 200 eV with 1 eV increments. High resolution scans for carbon and sulfur were collected with pass energy of 50 eV with 0.1 eV increments.

Atomic force microscopy (AFM) images were obtained on P3HT:PS thin films using a Bruker Dimension Icon AFM in tapping mode with n-type silicon tips (HQ:NSC14/NoAl, 160 kHz, 5 N/m, MikroMasch).

Fourier transform infrared spectroscopy (FTIR) was performed on free-standing films using a Nicolet 6700 FT-IR spectrometer (Thermo Fisher) in transmission mode. Each spectrum was collected with 8 scans and baseline corrected prior to analysis. PP:PS calibration films were measured with 9 replicates at different film positions.

Microscope images were taken using a Renishaw inVia Confocal Microscope. Films were imaged using a 5X objective lens, and a high-resolution film scan was stitched using a montage of 5X images taken in a grid across the sample.

3. RESULTS AND DISCUSSION

Tracer Studies

The passive herringbone mixer was central to enabling composition gradient thin films, as it is the flow module responsible for controlling the effluent mixture ratio of the analyte solutions of interest. To provide for robust control of the outlet composition profile, tracer studies were performed to elucidate the sensitivity of the time-dependent concentration of the effluent stream with respect to a given flow input. These RTD measurements also served as a diagnostic tool to assess the general mixing behavior of the coating system. A key success metric in the design is the ability to reliably characterize a coated film with a distribution of compositions between desired endpoints. The 30:70 P3HT:PS was selected as the vehicle for tracer studies because the solution concentration can be easily quantified through UV-vis absorption measurements. P3HT:PS also serves as a representative conjugated polymer system, which is of interest in the broader field of organic electronics and film composition/processing/morphology is known to impact performance.[50] Subsequently, deposited P3HT:PS thin films allow spectroscopic verification of the as-cast composition and display structural motifs that can be morphologically characterized with spatially resolved techniques such as AFM.

Figure 2a shows a representative RTD tracer signal using a pulse input, which directly characterizes the fluid mixing behavior of polymer species flowing through the staggered herringbone mixer. Tracer data was fit to two different models: (1) a TIS model fitting the mixing behavior between CSTR and PFR behavior, and (2) a MBM model that accounts for non-ideal mixing behavior. The non-ideal effects include bypassing and dead volume (*i.e.*, a volume fraction of species exit at a residence time lower or higher, respectively, than a majority of the species) that could be present in herringbone mixers and potentially affect mixer performance.[28]

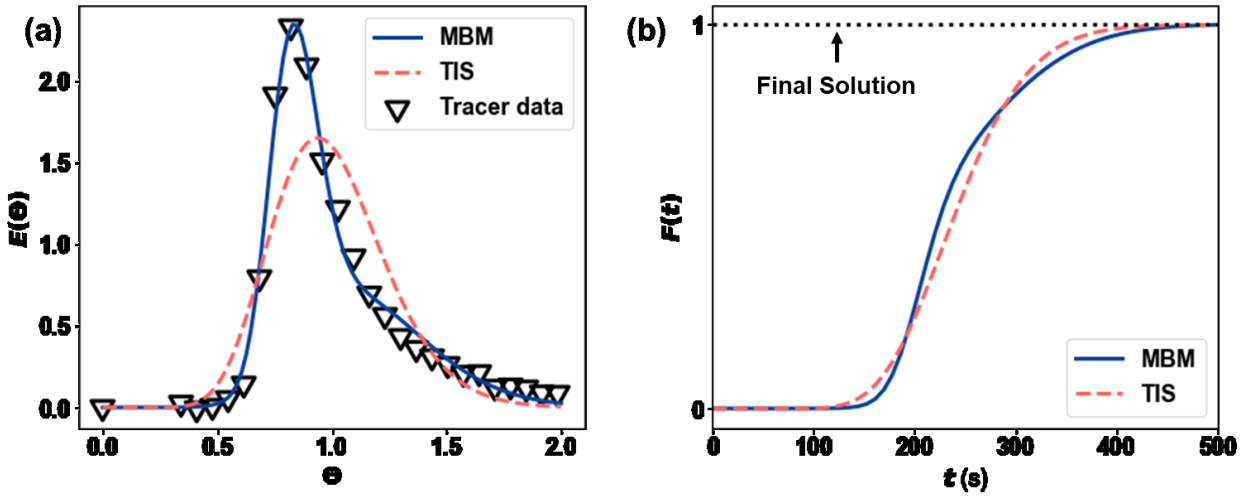

Figure 2. (a) Representative RTD data and model fits for Tank-in-Series (TIS) and Multibranch Model (MBM) derived from signal response to a 30:70 P3HT:PS pulse tracer input, (b) Prediction of effluent profile *F(t)* of a step input from initial to final solution at 20 mL/h, using model parameters from MBM and TIS pulse RTD fits.

Table 1. RTD model fit parameters for flow rates of 20, 60, and 100 mL/h using a 30:70 P3HT:PS tracer. Fits were performed on three replicate pulse tracer experiments for each flow rate. *Re* is the Reynolds number.

Q		TIS	MBM			
[mL/hr]	*Re*	*n*	*n*	*m*	*f*	*α*
20	**0.03**	13.4 ± 1.5	70.1 ± 3.5	16.2 ± 4.3	0.40 ± 0.03	1.40 ± 0.02
60	**0.09**	16.1 ± 1.6	57.8 ± 4.8	15.6 ± 2.1	0.51 ± 0.02	1.38 ± 0.03
100	**0.15**	15.4 ± 4.1	66.7 ± 11	14.5 ± 4.7	0.35 ± 0.04	1.35 ± 0.10

Table 2. Comparison of apparent and expected residence times for the employed herringbone mixer.

Q	τ_a	τ_0	$\frac{\tau_a}{\tau_0}$
[mL/hr]	[s]	[s]	
20	235.6	368.7	0.64
60	73.9	123	0.60

100	48.3	73.8	0.65

The presence of non-ideal mixing behavior in the passive mixer is apparent by inspection of the visual best fit of the tracer data to the MBM model over the ideal TIS model (**Figure 2a**). The one-parameter TIS equation models the behavior as a unimodal residence time distribution which is only sufficient in modeling the fluid elements represented by the main stream in the MBM model, as evidenced by the similarity in values between n in the TIS model and m in the MBM model. These parameters respectively model the number of equivalent CSTRs that describe the ideal mixing behavior (**Table 1**). The TIS model is visually imperfect in characterizing the mixer behavior as a significant portion of residence times are overpredicted for a volume of fluid elements. On the other hand, the multiparameter MBM equation is more accurate for the observed tracer behavior; further insight is provided by the model parameters. The values of $f \sim 0.35$-0.51 indicate the presence of a non-ideal side stream that makes up a significant fraction of the total fluid flow and signals a departure from TIS, while $\alpha > 1$ indicates the side stream is a result of bypass behavior. The presence of bypassing is further corroborated by the measured values of the apparent residence time (τ_a), which are consistently lower than the average expected residence time (τ_0) (**Table 2**) as calculated from the known mixer volume (Equation 3b). Additionally, the MBM fit effectively captures the narrower distribution of the bypassing fluid elements relative to the main stream, as $n > m$ for the MBM parameters. Finally, the minor variations in the fitted model parameters show that the flow rate does not significantly affect the dimensionless RTD profile across the range of flow rates studied (**Figure S2, Supporting Information**), allowing profiles at other flow rates within the same flow regime to be estimated.

Significant bypassing can introduce undesired plateaus or bimodalities to the concentration profile. As a result, the nonideal behavior raises the question of whether the herringbone mixer can reliably produce a gradient composition profile at the outlet. In practice, a full composition change between initial and final input solutions could take place through either a step input or a gradual ramp in flow rates. Here, the step input was employed to establish a gradient concentration profile in the effluent, as a gradual input change might be expected to consume more solution and substrate material. Using Equation (8) and the parameters in Table 1, **Figure 2b** presents the predicted concentration profile for both RTD models when a step input from initial to tracer solution is infused into the flow system at 20 mL/h. The RTD models then provide a useful tool to enable the outlet concentration of a step input to be spatially and temporally predictable. While this estimated gradient composition profile is not linear, linearity is not necessary to enable screening. However, the profiles should be monotonic in order to make efficient use of available solution volumes and space required to coat the substrate.

In the absence of nonideal mixing such as in the TIS model, the monotonic trend is unimpeded. As shown in **Figure 2b,** the predicted step profile for MBM also maintains monotonic behavior even though slight deviations are apparent. The behavior is reflected in the tracer profile; although the MBM tracer fit indicates the presence of a side stream, the average residence times of the main and side streams are similar ($\alpha \sim 1.4$): the RTD profile does not exhibit bimodal behavior, as might be the case for $\alpha > 5$.[47] Overall, the TIS and MBM models predict a similar composition profile, within experimental uncertainties.

Ambient Temperature Demonstration

To determine the agreement with the predicted step profile, gradient thin films were deposited and directly measured using P3HT:PS. **Figure 3** displays measurements performed on a deposited P3HT:PS gradient thin film coated at a flow rate of 20 mL/h and a step input flow profile from a 0 wt.% to a 30 wt.% P3HT solution. According to the prediction in **Figure 2b**, there is an initial time delay before the first P3HT-rich species exits the mixer. This prediction provided key information needed to purge the initial volume of effluent, avoiding the coating of excess uniform composition film on the substrate. The start of the film coating was then synchronized to take place just prior to the onset of effluent composition increase (at about 140 s) to capture relevant behavior from both models (TIS predicts the composition increase occurs slightly sooner). Note that at a stage translation speed of 2.5 mm/s, most of the expected concentration increase would be coated across 300-400 mm of the substrate. Given that this exceeded the length constraints of the translation stage in the present study, the gradient film sample measured in **Figure 3** was coated over successive substrates by iteratively pausing flow operation and resetting the stage position. While the low values of *Re* (**Table 1**) imply negligible changes in the internal concentration profile inside the mixer when this pause in operation occurs, long mixer residence times can either be seen as an advantage for studying finer changes in composition or an inconvenience when lesser human intervention is desired. This drawback could potentially be accounted for by designing a set of mixer options of varying mixer volume that could be interchanged depending on the requirements of the solution.

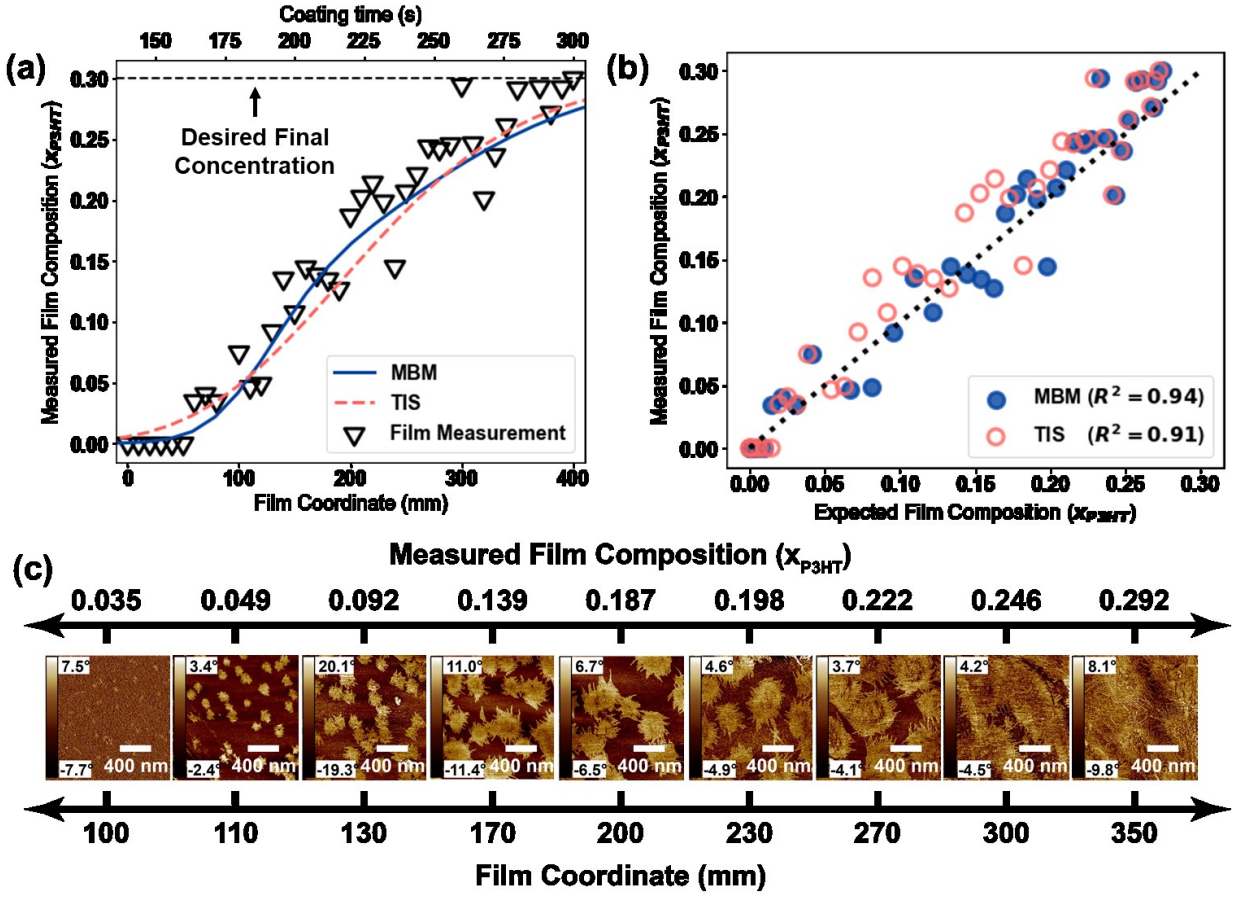

Figure 3. Characterization of a composition gradient film cast from P3HT:PS in chloroform solution by using a step input at 20 mL/hr. (a) Film composition measurements taken from XPS

using the S2p peak (**Figure S3, Supporting Information**) along the coated film length. Upper abscissa is the elapsed time after the P3HT-rich solution is pumped as the step input, where the mixer effluent was purged for 140 seconds prior to flow diversion to the coating stage. Colored lines represent the expected composition of the outlet as predicted by integration of RTD models (MBM = Multibranch; TIS = Tank-in-Series), and black dashed line represents the P3HT-rich composition or expected composition with $t \rightarrow \infty$. (b) Parity plot between RTD-predicted film composition and measured film composition. (c) Tapping-mode AFM phase images at selected points along the film coordinate of the P3HT:PS gradient film.

XPS characterization (**Figure 3a**) validated the predicted gradient composition profile with the as-cast thin films. As with solution-state tracer studies, the MBM step profile is a better visual fit to the thin-film experimental results. At low compositions, TIS overpredicts the deposited film composition; MBM more accurately predicts when the first fluid elements of tracer solution exit onto the substrate; measurements at lower film coordinates exhibit lower errors with MBM. At intermediate compositions, the TIS model tends to slightly underpredict film composition, which aligns with the observation of slight bypass behavior in the initial tracer studies. However, both models exhibit $R^2 > 0.90$, which indicates an acceptable level of error with which either RTD model prediction can inform an intended composition profile (**Figure 3b**). Akaike Information Criterion (AIC) value comparison favors the TIS model, as the improved prediction in MBM requires 3 additional model parameters (**Table S1, Supporting Information**). Therefore, while non-ideal mixing behavior is observed in the mixer, its presence does not significantly affect the desired monotonic trend desired for the composition gradient profile.

The surface morphology change over a P3HT gradient film composition window between 0 wt.% and 30 wt.% was interrogated using AFM (**Figure 3c**). The lowest P3HT compositions ($0 < x_{P3HT} < 0.10$) are associated with an initial appearance of P3HT droplets, which grow into larger fibrillar domains that approach diameters of $\sim 10^2$ nm ($0.10 < x_{P3HT} < 0.20$). At compositions approaching $x_{P3HT} = 0.30$, P3HT domains appear to overlap and evolve into a more continuous fibrillar network. This behavior aligns with the observations by Chang et al. in a study which correlated a similar morphological behavior in P3HT:PS to a plateau in charge carrier mobility between $0 < x_{P3HT} < 0.30$.[43] The ability to interrogate spectroscopic and morphological behavior demonstrates the utility of this approach to screen multicomponent space for the sake of materials discovery. Exploration of other systems using a variety of characterization techniques could also be envisioned to interrogate the composition/process space of blends for a range of organic electronics applications.

Additionally, the agreement between the predicted composition from solution-state RTD modeling and the measured composition from corresponding thin-film measurements helps to validate the reported protocol for generating compositional thin-film libraries. Hence, we have demonstrated the utility of modeling the mixing behavior within our coating system to optimize the gradient film deposition process. While previous studies have reported models to characterize mixing, non-ideal effects such as dead space and bypassing that might exist in microfluidic systems have not been considered.[28] As a result, predictions would be inaccurate leading to missed opportunities in rendering more efficient sample generation. For example, Basak *et al.* incorporated a transient mass balance model to inform gradient profiles but relied on a perfect mixing assumption that may not be universally extensible to other coating designs.[19] Where models are unavailable or unreported, composition is modulated using gradual, linear changes in

the relative flow rates of the inlet solutions to avoid departure from perfect mixing assumptions.[18] These gradual flow rate changes, however, lead to longer coating times or large substrate length requirements.[19, 36] As demonstrated in our results, modeling mixer behavior validates the ability of a step input to efficiently produce a gradient profile. These results are expected to provide an example of how RTD studies can enable the efficient design of other gradient coating systems and processes.

Elevated Temperature Demonstration

To enable the high-throughput experimentation of polymer systems that exhibit limited solubility, library generation via elevated temperature deposition is desirable. To accommodate elevated temperature operation, the herringbone mixer was implemented in aluminum. Further, syringes were constructed of stainless steel with solvent resistant O-rings that can hold pressure necessary to balance solvent vapor pressure at elevate temperature. PP was selected to demonstrate this feature because it is insoluble in benign solvents at ambient temperatures: the solution processing of PP requires elevated temperature dissolution in a small set of possible solvents, many of which are harsh chemicals and have relatively high boiling points (*e.g.*, xylene, decalin, tetralin, trichlorobenzene).[51]

A variety of commercial end uses are afforded by blending PP with a variety of fillers or other polymers in ratios that can accordingly tune the desired thermal, mechanical, or morphological properties of the final blend.[52] For example, the widespread availability of both PP and PS motivates the exploration of PP:PS blends to engineer materials with a range of uses.[53] Since the strong immiscibility of PP and PS hampers the mechanical performance of PP:PS,[54] low percentages (<5-10 wt.%) of compatibilizers such as maleic anhydride-grafted polypropylene (MA-g-PP)[55] or styrene-ethylene-butylene-styrene (SEBS)[56] are often incorporated into these blends to mitigate phase separation.[57] Therefore, efficiently screening of the phase behavior of the compatibilized PP:PS blend space is important in understanding the compositional and morphological effects on the thin-film properties. Thus, the system represents a model polymer blend to demonstrate the elevated temperature operation of the gradient film coating methodology developed here.

To generate PP:PS gradient films for this demonstration, MA-g-PP was used as the compatibilizer and o-xylene (boiling point 144 °C) was selected as the solvent. MA-g-PP was required because in the absence of a compatibilizer, free-standing PP:PS films at intermediate blend ratios underwent delamination due to complete phase separation during the film drying process. The solvent, o-xylene, proved effective in solubilizing PP at elevated temperatures in the concentration range of interest for thin film fabrication. The operating temperatures of the metal syringes, coating system, and stage were maintained at 110 °C. This temperature was sufficiently high to ensure the polymers would remain dissolved inside the coating system, while avoiding leakage at the outlet caused by vapor pressure effects from o-xylene observed at operating temperatures ~125 °C and higher. For other materials systems, this operating window will vary and is loosely bounded by the polymer solubility temperature and the solvent boiling point. Like many thin-film systems, the compatibilized PP:PS blend system employed here exhibited FTIR-detectable spectroscopic changes. While FTIR was primarily used to measure thin-film composition, it could also be adapted to rapidly screen molecular changes with respect to library coordinates. Selected peak area features, which were measured on a series of compatibilized PP:PS

samples of known, uniform blend fraction, were used to calibrate composition measurements (**Figure S4, Supporting Information**).

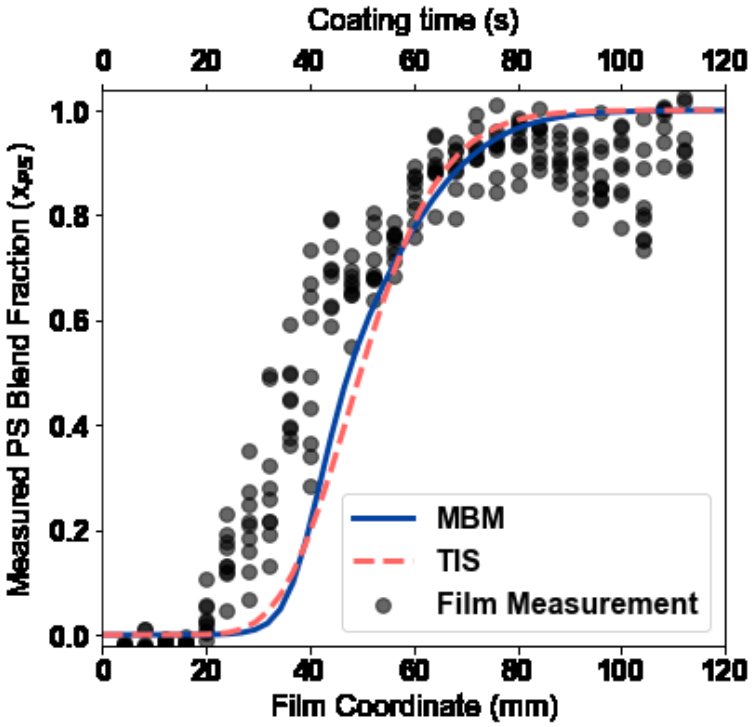

Figure 4. Composition profile of deposited PP:PS + 5 wt.% MA-g-PP gradient film coated from a step-input flow profile from PP + 5 wt.% MA-g-PP (x_{PS} = 0) to PS + 5 wt.% MA-g-PP (x_{PS} = 1.0). Solid and dashed lines are modeled composition profiles as predicted from P3HT:PS tracer studies (MBM = Multibranch; TIS = Tank-in-Series).

RTD models were employed to provide a predicted composition profile for MA-g-PP compatibilized PP:PS gradient film coating by using a step input from an initial x_{PS} = 0 to x_{PS} = 1.0 (**Figure 4**). Several FTIR measurements were taken to provide a representative local distribution of compositions along each lateral coordinate. The resulting distribution of film compositions generally aligned with the predicted step response, though the mean expected compositions were slightly underpredicted at early time steps. The deviation, while small, from the P3HT:PS tracer model suggests that a fraction of the species spends less time in the overall flow system. This is likely explained by the lower viscosity of the PS-rich solution relative to the PP-rich solution, which may cause a small amount of the PS-rich component bypassing in the mixer and result in lower residence times (**Table S2, Supporting Information**).

While the mean composition of multiple measurements taken along the same lateral coordinate in (**Figure 4)** falls near the expected trend given by the RTD models, the actual measured composition may vary across the width of the film. Variance of the measured composition across the film width at a given 'constant composition' position is most notable at intermediate blend ratios. Phase separation is most likely the greatest contributor to these fluctuations. A small amount of variation might also be attributed to minute thickness differences

between the top or bottom edges of the film, which could be caused by slight blade misalignment or stage leveling. Such thickness variations may cause small differences in the entropic contribution to the energy of mixing, possibly leading to minor changes in phase behavior.

An ideal library sample would generate a distribution of intermediate compositions along the sample width between the two desired endpoints (*i.e.*, $x_{PS} = 0$ (PP-rich) and $x_{PS} = 1.0$ (PS-rich)) in as few individual substrates as possible, to improve efficiency in resource usage and reduce the characterization workload. While the composition step profile (**Figure 4**) was coated upon two substrates of 60 mm of film length each, portions of the coating consisted of film area of near-constant composition. Based on the data and the RTD models, the greatest composition increase takes place between 20-80 mm. This processing window was used to separately deposit a continuous gradient film on a single substrate to spatially characterize the morphology of the compatibilized PP:PS composition space (**Figure 5**).

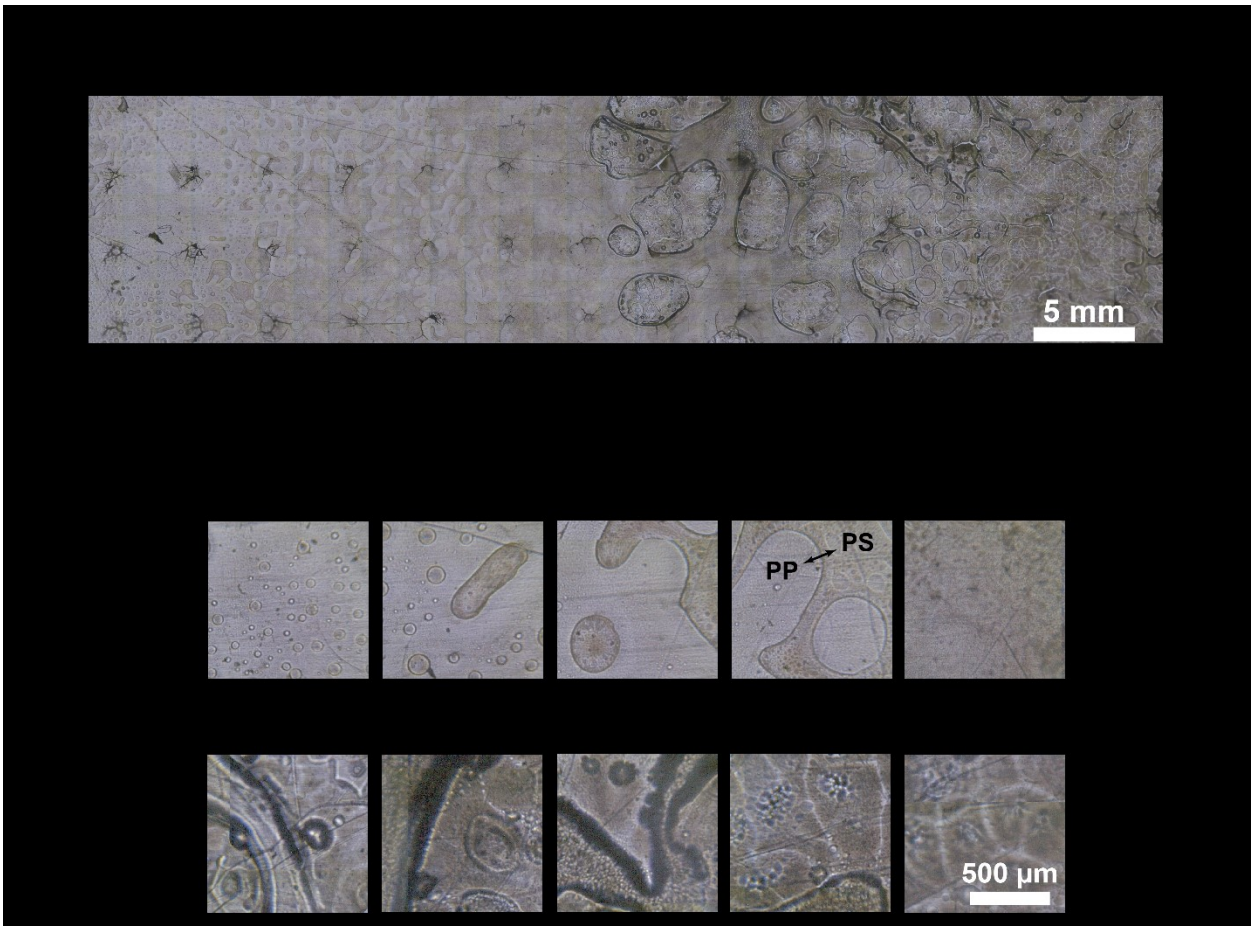

Figure 5. (a) Stitched montage of 5X optical images mapping the film morphology of a single MA-g-PP compatibilized PP:PS gradient film deposited using continuous infusion of a step input. Images were collected after mechanical testing (HTMECH), so that the comparative length scale of holes created by the mechanical force sensor is depicted. Measured polystyrene composition is reported as the average of nine calibrated FTIR measurements at 2-mm intervals along the vertical axis of the image. (b) 5x images cropped from higher resolution montage along selected film coordinates.

Figure 5 demonstrates the evolution of phase behavior as the PS blend fraction (x_{PS}) progresses along the gradient film length. Lower loadings of PS are characterized by the appearance of PS droplets (confirmed through hyperspectral imaging, **Figure S5, Supporting Information**) that increase in size until an evolution into a bicontinuous phase morphology up through $x_{PS} \sim 0.40–0.50$. At intermediate values of x_{PS} above 0.50, incomplete phase separation occurs with the appearance of large spherical PS-rich domains that exceed the millimeter length scale. These globular domains ultimately evolve into a more "cellular" PS-rich phase at higher PS blend fractions, where individual PS-rich cells appear to be separated by what could be MA-g-PP/PP-rich boundaries.

High-throughput mechanical property screening on the same library sample was also performed. Thin film mechanical properties were significantly impaired (low tensile strength and strain at break) above the $x_{PS} \sim 0.50$ threshold (**Figure S6, Supporting Information**). The results agree with the morphological behavior as evidenced by the large phase boundaries that were observed due to PP and PS immiscibility at higher blend fractions. Additionally, this morphological behavior and associated mechanical trend agrees with the findings by Parameswaranpillai et al., who reported a similar morphological/mechanical relationship for MA-g-PP compatibilized PP:PS using coarse x_{PS} ratio intervals of 0.20. In contrast to a one-at-a-time sampling approach of equally spaced, individual uniform composition films, the gradient library approach allows for more comprehensive screening of the major phase transitions within the composition space. The results presented here, which quickly rule out larger x_{PS} formulations that might require mechanical tunability/performance, serve as a preliminary high-throughput screening for the compatibilized PP:PS system. The gradient libraries shown above could feasibly be generalized to explore the composition space of other blends, compatibilizers, molecular weights, and/or processing temperatures within PP formulations.

4. CONCLUSIONS

Here, a methodology for generating composition gradient thin-film libraries *via* a system incorporating a metallic passive herringbone mixer and elevated temperature capabilities is presented. It was demonstrated that quantification of mixer behavior permits the rational selection of flow inputs and coating parameters for a plethora of analytes. To this end, RTD modeling was employed as a key component of the protocol. Integrated with the judiciously designed coating system, we showed that this effluent profile control enabled the compositional screening of both ambient (P3HT:PS) and elevated temperature (PP:PS) materials systems.

We envision that the methodology presented here will enable the study of a wider breadth of solution processed, multicomponent materials, particularly where elevated temperature and mixer design considerations are mandatory to achieve solubility and/or processible viscosity. These capabilities are of interest for accelerating the discovery and/or process optimization of contemporary materials of research interest, including organic electronics, colloidal nanocrystals, photoactive polymers, separations membranes, polyolefins, and many more. The approach, which incorporates RTD analysis, could also be extended to enable library generation for other process platforms where residence times can be measured (*e.g.*, other solution-based coating systems, flow reactors, melt extrusion, etc.). Given increasing community interest in autonomous experimentation, machine learning, and data-driven materials science, our demonstration provides considerations for others interested in designing custom sampling methods toward high-

throughput experimentation. By broadly leveraging the techniques reported herein, the informatics-driven experimentation of many materials systems is expected to be accelerated.

ASSOCIATED CONTENT

Supporting Information

The Supporting Information is available free of charge online.

Additional experimental details; UV-vis spectra for representative tracer experiments, sample RTD profiles from all flow rates; XPS survey scan profile for P3HT:PS thin film; FTIR signatures and calibration for PP:PS samples, FTIR microscopy for PP:PS gradient film; High-throughput mechanical characterization of PP:PS gradient film

AUTHOR INFORMATION

Corresponding Authors

Elsa Reichmanis – Chemical & Biomolecular Engineering, Lehigh University, Bethlehem, PA

Martha A. Grover – School of Chemical & Biomolecular Engineering, Georgia Institute of Technology, Atlanta, GA, 30332

Carson Meredith – School of Chemical & Biomolecular Engineering, Georgia Institute of Technology, Atlanta, GA, 30332

Other Authors

Aaron L. Liu – School of Chemical & Biomolecular Engineering, Georgia Institute of Technology, Atlanta, GA, 30332

Ezgi M. Dogan-Guner – School of Chemical & Biomolecular Engineering, Georgia Institute of Technology, Atlanta, GA, 30332; current address, Institute for Surface Technology, Technische Universität Braunschweig, D 38108 Braunschweig, Germany

Michael McBride – School of Chemical & Biomolecular Engineering, Georgia Institute of Technology, Atlanta, GA, 30332; current address, Los Alamos National Laboratory, Los Alamos, NM 87545

Rahul Venkatesh – School of Chemical & Biomolecular Engineering, Georgia Institute of Technology, Atlanta, GA, 30332

Miguel Angel Gonzalez – School of Chemical & Biomolecular Engineering, Georgia Institute of Technology, Atlanta, GA, 30332

ORCID:

Aaron L. Liu: 0000-0001-7347-5347
Miguel A. Gonzalez: 0000-0002-2554-4149
Elsa Reichmanis: 0000-0002-8205-8016
Martha Grover: 0000-0002-7036-776X
J. Carson Meredith: 0000-0003-2519-5003
Michael McBride: 0000-0002-5274-7275
Ezgi M. Dogan-Guner: 0000-0002-4647-6114
Rahul Venkatesh: 0000-0003-1008-6568

Notes

The authors declare no conflict of interest.

ACKNOWLEDGMENTS

Financial support from NSF DMREF (Grant No. 1922111, DMREF: Collaborative Research: Achieving Multicomponent Active Materials through Synergistic Combinatorial, Informatics-Enabled Materials Discovery) toward RTD modeling and P3HT:PS gradient film studies is gratefully acknowledged. Funding from Konica Minolta Laboratory USA is appreciated for supporting the work related to polypropylene discovery. Bradley Parker is gratefully acknowledged for technical support in the mixer and distributor design. Guoyan Zhang and Jiaxi Xu are acknowledged for contributing foundational knowledge for solution processing and tracer studies, respectively. Rallming Yang, Anna Osterholm, and Wenting Shi are acknowledged for their assistance with supporting measurements for PP:PS work. Zihao Qu at Georgia Tech provided an early design of the herringbone mixer design. This work was performed in part at the Georgia Tech Institute for Electronics and Nanotechnology, a member of the National Nanotechnology Coordinated Infrastructure, which is supported by the National Science Foundation (ECCS-1542174).

REFERENCES

1. Blatt, M. P.; Hallinan, D. T., Polymer Blend Electrolytes for Batteries and Beyond. *Industrial & Engineering Chemistry Research* **2021,** *60* (48), 17303-17327.
2. Li, M.; Igbari, F.; Wang, Z. K.; Liao, L. S., Indoor Thin-Film Photovoltaics: Progress and Challenges. *Advanced Energy Materials* **2020,** *10* (28), 2000641.
3. Xie, K.; Fu, Q.; Qiao, G. G.; Webley, P. A., Recent progress on fabrication methods of polymeric thin film gas separation membranes for CO2 capture. *Journal of Membrane Science* **2019,** *572*, 38-60.
4. Zhao, C.; Li, L.-Y.; Guo, M.-M.; Zheng, J., Functional polymer thin films designed for antifouling materials and biosensors. *Chemical Papers* **2012,** *66* (5), 323-339.
5. Pan, Y.; Yu, G., Multicomponent Blend Systems Used in Organic Field-Effect Transistors: Charge Transport Properties, Large-Area Preparation, and Functional Devices. *Chemistry of Materials* **2021,** *33* (7), 2229-2257.
6. Wang, Y.; Li, Z.; Xiao, J., Stretchable Thin Film Materials: Fabrication, Application, and Mechanics. *Journal of Electronic Packaging* **2016,** *138* (2), 020801.
7. Syafiq, R. M. O.; Sapuan, S. M.; Zuhri, M. Y. M.; Othman, S. H.; Ilyas, R. A., Effect of plasticizers on the properties of sugar palm nanocellulose/cinnamon essential oil reinforced starch bionanocomposite films. *Nanotechnology Reviews* **2022,** *11* (1), 423-437.
8. Kang, B.; Ge, F.; Qiu, L.; Cho, K., Effective Use of Electrically Insulating Units in Organic Semiconductor Thin Films for High-Performance Organic Transistors. *Advanced Electronic Materials* **2017,** *3* (2). 1600240
9. Nam, M.; Lee, C.; Ko, D.-H., Sequentially processed quaternary blends for high-performance indoor organic photovoltaic applications. *Chemical Engineering Journal* **2022,** *438*. 135576
10. Ivancic, R. J. S.; Riggleman, R. A., Dynamic phase transitions in freestanding polymer thin films. *Proc Natl Acad Sci U S A* **2020,** *117* (41), 25407-25413.
11. Meredith, J. C.; Karim, A.; Amis, E. J., High-Throughput Measurement of Polymer Blend Phase Behavior. *Macromolecules* **2000,** *33* (16), 5760-5762.
12. Potyrailo, R.; Rajan, K.; Stoewe, K.; Takeuchi, I.; Chisholm, B.; Lam, H., Combinatorial and high-throughput screening of materials libraries: review of state of the art. *ACS Comb Sci* **2011,** *13* (6), 579-633.
13. Genzer, J., Surface-Bound Gradients for Studies of Soft Materials Behavior. *Annual Review of Materials Research* **2012,** *42* (1), 435-468.
14. Materials Genome Initiative. https://www.mgi.gov/ (accessed 2022-03-24).
15. Green, M. L.; Choi, C. L.; Hattrick-Simpers, J. R.; Joshi, A. M.; Takeuchi, I.; Barron, S. C.; Campo, E.; Chiang, T.; Empedocles, S.; Gregoire, J. M.; Kusne, A. G.; Martin, J.; Mehta, A.; Persson, K.; Trautt, Z.; Van Duren, J.; Zakutayev, A., Fulfilling the promise of the materials genome initiative with high-throughput experimental methodologies. *Applied Physics Reviews* **2017,** *4* (1), 011105.
16. Baudis, S.; Behl, M., High-Throughput and Combinatorial Approaches for the Development of Multifunctional Polymers. *Macromol Rapid Commun* **2021**, e2100400.
17. Rodriguez-Martinez, X.; Pascual-San-Jose, E.; Campoy-Quiles, M., Accelerating organic solar cell material's discovery: high-throughput screening and big data. *Energy Environ Sci* **2021,** *14* (6), 3301-3322.
18. Alstrup, J.; Jorgensen, M.; Medford, A. J.; Krebs, F. C., Ultra fast and parsimonious materials screening for polymer solar cells using differentially pumped slot-die coating. *ACS Appl Mater Interfaces* **2010,** *2* (10), 2819-27.
19. Basak, P.; Zapata, P.; Reed, K.; Gomez, I.; Meredith, J. C., Continuous Infusion Microchannel Approach to Generate Composition Gradients from Viscous Polymer Solutions. In *Soft Matter Gradient Surfaces: Methods and Applications*, Genzer, J., Ed. Wiley: New York, 2012; pp 129-143.
20. Gomez, I. J.; Wu, J.; Roper, J.; Beckham, H.; Meredith, J. C., High Throughput Screening of Mechanical Properties and Scratch Resistance of Tricomponent Polyurethane Coatings. *ACS Applied Polymer Materials* **2019,** *1* (11), 3064-3073.
21. Rodríguez-Martínez, X.; Sevim, S.; Xu, X.; Franco, C.; Pamies-Puig, P.; Córcoles-Guija, L.; Rodriguez-Trujillo, R.; Campo, F. J.; Rodriguez San Miguel, D.; deMello, A. J.; Pané, S.; Amabilino, D. B.; Inganäs, O.; Puigmartí-Luis, J.; Campoy-Quiles, M., Microfluidic-Assisted Blade Coating of Compositional Libraries for Combinatorial Applications: The Case of Organic Photovoltaics. *Advanced Energy Materials* **2020,** *10* (33), 2001308.

22. Lee, C.-Y.; Wang, W.-T.; Liu, C.-C.; Fu, L.-M., Passive mixers in microfluidic systems: A review. *Chemical Engineering Journal* **2016,** *288*, 146-160.
23. Roy, A. L.; Chiu, H. N.; Walus, K., A microfluidic-enabled combinatorial formulation and integrated inkjet printing platform for evaluating functionally graded material blends. *Lab Chip* **2021,** *21* (22), 4427-4436.
24. Love, J. C.; Anderson, J. R.; Whitesides, G. M., Fabrication of Three-Dimensional Microfluidic Systems by Soft Lithography. *MRS Bulletin* **2011,** *26* (7), 523-528.
25. Ward, K.; Fan, Z. H., Mixing in microfluidic devices and enhancement methods. *J Micromech Microeng* **2015,** *25* (9), 094001.
26. Lee, C.-Y.; Chang, C.-L.; Wang, Y.-N.; Fu, L.-M., Microfluidic mixing: a review. *Int J Mol Sci* **2011,** *12* (5), 3263-3287.
27. Aubin, J.; Fletcher, D.; Bertrand, J.; Xuereb, C., Characterization of Mixing Quality in Micromixers. *Chemical Engineering & Technology* **2003,** *26*, 1262-1270.
28. Ianovska, M. A.; Mulder, P. P. M. F. A.; Verpoorte, E., Development of small-volume, microfluidic chaotic mixers for future application in two-dimensional liquid chromatography. *RSC Advances* **2017,** *7* (15), 9090-9099.
29. Stroock, A. D.; Dertinger, S. K.; Ajdari, A.; Mezic, I.; Stone, H. A.; Whitesides, G. M., Chaotic mixer for microchannels. *Science* **2002,** *295* (5555), 647-51.
30. Tóth, E.; Holczer, E.; Iván, K.; Fürjes, P., Optimized Simulation and Validation of Particle Advection in Asymmetric Staggered Herringbone Type Micromixers. *Micromachines* **2014,** *6* (1), 136-150.
31. Giri, K.; Tsao, C. W., Recent Advances in Thermoplastic Microfluidic Bonding. *Micromachines (Basel)* **2022,** *13* (3), 486.
32. Niklaus, F.; Stemme, G.; Lu, J. Q.; Gutmann, R. J., Adhesive wafer bonding. *Journal of Applied Physics* **2006,** *99* (3), 031101.
33. Radadia, A. D.; Salehi-Khojin, A.; Masel, R. I.; Shannon, M. A., The fabrication of all-silicon micro gas chromatography columns using gold diffusion eutectic bonding. *Journal of Micromechanics and Microengineering* **2010,** *20* (1), 015002.
34. Iliescu, C.; Taylor, H.; Avram, M.; Miao, J.; Franssila, S., A practical guide for the fabrication of microfluidic devices using glass and silicon. *Biomicrofluidics* **2012,** *6* (1), 16505-1650516.
35. Bormashenko, E.; Pogreb, R.; Musin, A.; Stanevsky, O.; Bormashenko, Y.; Whyman, G.; Gendelman, O.; Barkay, Z., Self-assembly in evaporated polymer solutions: influence of the solution concentration. *J Colloid Interface Sci* **2006,** *297* (2), 534-40.
36. An, N. G.; Kim, J. Y.; Vak, D., Machine learning-assisted development of organic photovoltaics via high-throughput in situ formulation. *Energy & Environmental Science* **2021,** *14* (6), 3438-3446.
37. Nguyen, T.-Q.; Yee, R. Y.; Schwartz, B. J., Solution processing of conjugated polymers: the effects of polymer solubility on the morphology and electronic properties of semiconducting polymer films. *Journal of Photochemistry and Photobiology A: Chemistry* **2001,** *144* (1), 21-30.
38. Troshin, P. A.; Hoppe, H.; Renz, J.; Egginger, M.; Mayorova, J. Y.; Goryachev, A. E.; Peregudov, A. S.; Lyubovskaya, R. N.; Gobsch, G.; Sariciftci, N. S.; Razumov, V. F., Material Solubility-Photovoltaic Performance Relationship in the Design of Novel Fullerene Derivatives for Bulk Heterojunction Solar Cells. *Advanced Functional Materials* **2009,** *19* (5), 779-788.
39. Hu, X.; Zhou, L.; Gao, C., Hyperbranched polymers meet colloid nanocrystals: a promising avenue to multifunctional, robust nanohybrids. *Colloid and Polymer Science* **2011,** *289* (12), 1299-1320.
40. Zhou, H.; Jin, W., Membranes with Intrinsic Micro-Porosity: Structure, Solubility, and Applications. *Membranes (Basel)* **2018,** *9* (1), 3-30.
41. Chang, C. W.; Borne, I.; Lawler, R. M.; Yu, Z.; Jang, S. S.; Lively, R. P.; Sholl, D. S., Accelerating Solvent Selection for Type II Porous Liquids. *J Am Chem Soc* **2022,** *144* (9), 4071-4079.
42. Cook, J. G., *Handbook of polyolefin fibres*. Merrow Publishing Company: 1967.
43. Chang, M.; Choi, D.; Wang, G.; Kleinhenz, N.; Persson, N.; Park, B.; Reichmanis, E., Photoinduced Anisotropic Assembly of Conjugated Polymers in Insulating Polymer Blends. *ACS Appl Mater Interfaces* **2015,** *7* (25), 14095-103.
44. Shubhra, Q. T. H.; Alam, A.; Quaiyyum, M. A., Mechanical properties of polypropylene composites. *Journal of Thermoplastic Composite Materials* **2011,** *26* (3), 362-391.
45. Teh, J. W.; Rudin, A.; Keung, J. C., A review of polyethylene–polypropylene blends and their compatibilization. *Advances in Polymer Technology* **1994,** *13* (1), 1-23.
46. Fogler, H. S., *Elements of chemical reaction engineering*. 4th ed ed.; Prentice Hall PTR: Upper Saddle River, NJ, 2006.

47. Himmelblau, D. M.; Bischoff, K. B., *Process Analysis and Simulation: Deterministic Systems*. John Wiley & Sons: New York, 1968.
48. Davis, M. E.; Davis, R. J., *Fundamentals of Chemical Reaction Engineering*. McGraw-Hill: New York, NY, 2003.
49. Virtanen, P.; Gommers, R.; Oliphant, T. E.; Haberland, M.; Reddy, T.; Cournapeau, D.; Burovski, E.; Peterson, P.; Weckesser, W.; Bright, J.; van der Walt, S. J.; Brett, M.; Wilson, J.; Millman, K. J.; Mayorov, N.; Nelson, A. R. J.; Jones, E.; Kern, R.; Larson, E.; Carey, C. J.; Polat, I.; Feng, Y.; Moore, E. W.; VanderPlas, J.; Laxalde, D.; Perktold, J.; Cimrman, R.; Henriksen, I.; Quintero, E. A.; Harris, C. R.; Archibald, A. M.; Ribeiro, A. H.; Pedregosa, F.; van Mulbregt, P.; SciPy, C., SciPy 1.0: fundamental algorithms for scientific computing in Python. *Nat Methods* **2020,** *17* (3), 261-272.
50. Persson, N. E.; Chu, P. H.; McBride, M.; Grover, M.; Reichmanis, E., Nucleation, Growth, and Alignment of Poly(3-hexylthiophene) Nanofibers for High-Performance OFETs. *Acc Chem Res* **2017,** *50* (4), 932-942.
51. Yang, M. C.; Perng, J. S., Camphene as a novel solvent for polypropylene: Comparison study based on viscous behavior of solutions. *Journal of Applied Polymer Science* **2000,** *76* (14), 2068-2074.
52. Chukov, N. A.; Ligidov, M. K.; Pakhomov, S. I.; Mikitaev, A. K., Polypropylene polymer blends. *Russian Journal of General Chemistry* **2017,** *87* (9), 2238-2249.
53. Kim, K. Y.; Ju, D. U.; Nam, G. J.; Lee, J. W., Ultrasonic Effects on PP/PS/Clay Nanocomposites during Continuous Melt Compounding Process. *Macromolecular Symposia* **2007,** *249-250* (1), 283-288.
54. Latreche, L.; Haddaoui, N.; Cagiao, M. E., The effect of various compatibilizers on thermal, mechanical, and morphological properties of polystyrene/polypropylene blends. *Russian Journal of Applied Chemistry* **2017,** *89* (10), 1713-1721.
55. Parameswaranpillai, J.; Joseph, G.; Chellappan, R. V.; Zahakariah, A. K.; Hameed, N., The effect of polypropylene-graft-maleic anhydride on the morphology and dynamic mechanical properties of polypropylene/polystyrene blends. *Journal of Polymer Research* **2015,** *22*, 2
56. Horák, Z.; Fořt, V.; Hlavatá, D.; Lednický, F.; Večerka, F., Compatibilization of high-impact polystyrene/polypropylene blends. *Polymer* **1996,** *37* (1), 65-73.
57. Krishnan, A. K.; George, T. S.; Anjana, R.; Joseph, N.; George, K. E., Effect of modified kaolin clays on the mechanical properties of polypropylene/polystyrene blends. *Journal of Applied Polymer Science* **2013,** *127* (2), 1409-1415.

For Table of Contents Only